Controllable surfactant-directed zeolitic-imidazolate-8 growth on swollen 2D zeolites

Cite as: APL Mater. 11, 031115 (2023); doi: 10.1063/5.0139673
Submitted: 22 December 2022 • Accepted: 25 January 2023 •
Published Online: 22 March 2023

Philip Netzsch, Romy Ettlinger, and Russell E. Morris[a]

AFFILIATIONS

EastChem School of Chemistry, University of St Andrews, North Haugh, St Andrews KY16 9ST, United Kingdom

Note: This paper is part of the Special Topic on Challenges and Perspectives in Materials Chemistry–A Celebration of Professor Sir Anthony K. Cheetham's 75th Birthday.
[a]**Author to whom correspondence should be addressed:** rem1@st-andrews.ac.uk

ABSTRACT

To meet society's need for more and more specialized materials, this work focuses on the preparation of porous metal–organic framework (MOF)–zeolite hybrid materials based on two 2D zeolites, namely, IPC-1P (Institute of Physical Chemistry - 1 Precursor) and the metal–organic framework ZIF-8 (Zeolitic Imidazolate Framework-8). Using the previously well-established assembly–disassembly–organization–reassembly method, the zeolite was (i) synthesized, (ii) hydrolyzed to a layered zeolite, (iii) the interlayer distance was increased using the swelling agent cetyltrimethylammonium chloride, and (iv) nanocrystals of ZIF-8 were grown stepwise on the zeolite surface but predominantly at the edges of the crystallites where the openings to the interlayer region are located. This selective MOF growth and attachment was facilitated by a combination of intercalation of the metal ions and the swelling agent between the zeolite layers. The influence of the solvent and the number of additional steps on the ZIF-8 growth on the zeolite was systematically investigated, and the synthesis protocol was successfully adapted to a further two-dimensional silicate RUB-18 (Ruhr-Universität Bochum - 18). This paves the way toward the controlled preparation of more MOF–zeolite hybrid materials, which might provide interesting properties for future applications.

I. INTRODUCTION

Modern society benefits tremendously from the long history of porous materials: from their initial use for medical purposes in ancient Egyptian societies, materials, such as charcoal, activated carbon, and zeolites, are being further and further developed for highly specialized applications in numerous industrial processes, e.g., for the separation of (toxic) gases, ion exchange and catalytic processes in oil refining, petrochemistry, and water treatment.[1] Zeolites, which are crystalline silicate-based microporous materials, have been especially utilized in the industry where a combination of their chemistry with porous topologies leads to unique physicochemical properties that have in turn allowed them to be exploited for various industrial separation and catalytic processes.[2] However, since the late 1990s, another class of crystalline metal–organic hybrid materials, namely metal–organic frameworks (MOFs), experienced exponential research growth, and already more than 100 000 MOF structures, have been synthesized.[3] MOFs comprise metal ions or metal cluster nodes linked by organic molecules. This difference in chemistry leads to some interesting advantages and disadvantages compared to their purely inorganic zeolite analog, e.g., MOFs provide higher (i) metal–organic chemical versatility, (ii) internal surface areas (≥7000 m^2/g), and (iii) pore tunability. As a result, MOFs hold great promise in a wide range of applications that are different from those traditionally dominated by zeolites, ranging from gas storage and separation, water harvesting, energy conversion and storage, and sensing to biomedicine, e.g., health-care, diagnosis, therapy, and theragnostic.[3,4]

Given their very complementary chemical properties and broadly similar topologies, combining the rich chemistry of MOFs

with that of zeolites could lead to MOF–zeolite hybrid materials that combine the individual strengths of both classes of solid, i.e., high thermal stability and high acidic properties for zeolites and high surface area and tunability for MOFs.[5] However, their rather different synthetic routes, which require harsh conditions at elevated temperatures for long periods of time and often the use of HF or NaOH for zeolites, in contrast to milder conditions for the coordination polymerization of MOFs, make *in situ* synthesis of MOF–zeolite hybrid materials extremely challenging. Thus, the main synthesis strategy for MOF zeolite materials so far has been to start from a pristine zeolite and grow MOFs on its surface.[5] Such methods often require a surface functionalization of the starting zeolite with terminal groups similar to the MOF linker molecules, such as –COOH[6,7] or imidazole groups.[8–10] Another approach to obtain MOF–zeolite hybrid materials might be to start with two-dimensional zeolites,[11,12] as these could be utilized in other hybrid materials, such as organic pillared zeolites.[13–16] Besides the direct synthesis, two-dimensional zeolites can also be derived by the "top down" approach by disassembling a three-dimensional zeolite as part of the previously established Assembly–Disassembly–Organisation–Reassembly (ADOR) method.[17,18] The Ge-UTL zeolite represents a good model example since the germanium oxygen bonds in the Ge-rich double four ring units (D4R) can be hydrolyzed, and the material disassembled into the lamellar zeolite precursor IPC-1P (Institute of Physical Chemistry - 1 Precursor). Subsequently, the interlayer distance can be easily manipulated, and the chemistry is modified by swelling the zeolite with a surfactant, such as a cetyltrimethylammonium chloride (CTMA-Cl) to yield IPC-1sw (swollen). This makes the interlayer space more accessible for small molecules/ions to penetrate, and thus, hybrid materials, such as pillared layered zeolites, can be obtained.[14,19,20] Such modified two-dimensional zeolite precursors might be a good starting point for further hybrid materials, such as MOF–zeolite compounds. In this study, we focus on pushing the boundaries of ADOR-derived zeolites toward MOF–zeolite hybrid materials and preparing a zeolitic material that is decorated with MOF nanoparticles. To showcase this, one of the best-known MOF structures, namely ZIF-8 (Zeolitic Imidazolate Framework-8), was selected. For such hybrid materials, it is essential to be able to precisely control MOF growth in terms of size and morphology.[9,21] Herein, we develop a precise synthesis protocol to achieve a controllable, size, and morphology specific deposition of ZIF-8 nanoparticles on IPC-1sw by depending on different solvents and growth cycles. We show that we can control the predominant location of MOF growth, targeting the faces of the layered zeolite crystallites where the opening to the interlayer spaces is. Moreover, we could highlight the robustness of our optimized synthetic conditions by successfully transferring them to another 2D silicate, namely Na-RUB-18 (Ruhr-Universität Bochum - 18).

II. RESULTS AND DISCUSSION

A. IPC-1sw@ZIF-8

The lamellar zeolite precursor IPC-1P was derived from the parent Ge-UTL zeolite by hydrolysis according to the first step of the ADOR method (Scheme 1).[17] Subsequently, the material is swollen with the surfactant CTMA-Cl in order to yield the swollen zeolite IPC-1sw. In order to grow ZIF-8 on IPC-1sw, a two-step process was employed (Scheme 1). First, the swollen zeolite IPC-1sw was dispersed in a 0.1M Zn^{2+} aqueous solution so that the metal ions are intercalated between the zeolitic layers, balancing the charge of the deprotonated silanol groups. Any excess Zn^{2+} ions were removed by washing with water to prevent any unattached ZIF-8 particles from forming alongside the zeolite. Second, the Zn-loaded ICP-1sw was soaked in a 0.1M 2-methylimidazole (2-MeIm) solution. Herein, a

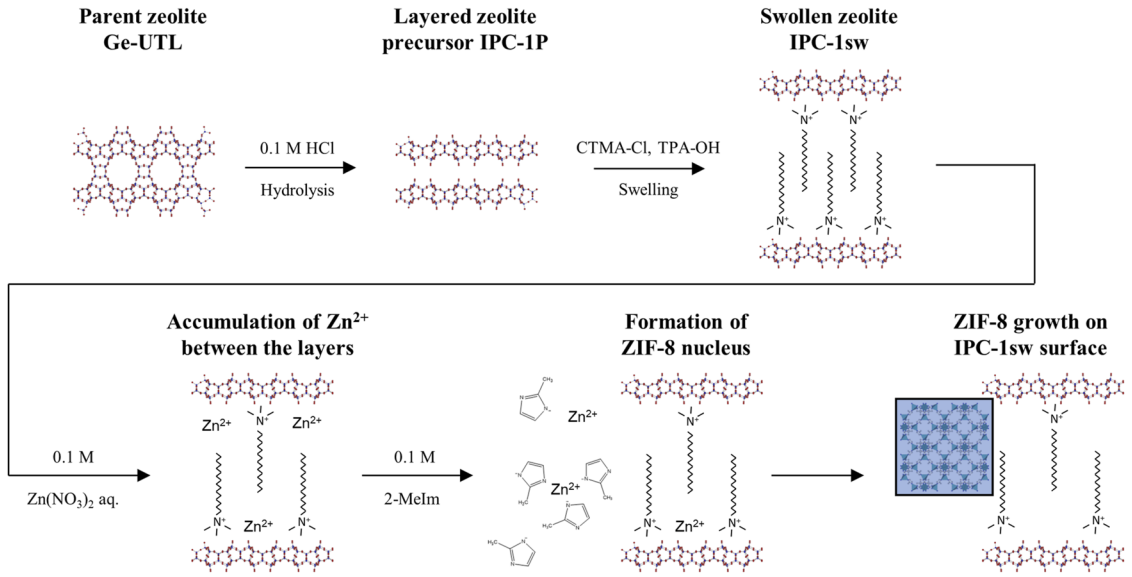

SCHEME 1. (Top) The ADOR synthesis of IPC-1P by the selective hydrolysis of zeolite Ge-UTL followed by swelling to form IPC-1sw. (Bottom) Synthesis protocol starts with the accumulation of Zn^{2+} between the layers, the formation of the ZIF-8 nucleus, and the growth of ZIF-8 nanoparticles attached to IPC-1sw.

H_2O:MeOH ratio of 9:1 turned out to be ideal to allow a moderate growth speed of ZIF-8 on the swollen zeolite IPC-1sw.

The powder x-ray diffraction (PXRD) pattern [Fig. 1(a)] shows the unchanged swollen structure of IPC-1sw, with the retention of the low angle reflection indicating the retention of the interlayer distance as well as the intralayer reflection at higher 2θ values.[22] The presence of crystalline ZIF-8 particles can be confirmed by the reflections at 2θ = 3.4°, 4.8°, 5.8°, 6.2°, 7.5°, and 8.2° (Mo-K_α). Furthermore, the FT-IR spectrum [Fig. 1(b)] shows the bands of the zeolite framework (1400–400 cm^{-1}), the presence of the $CTMA^+$ ions at 2920, 2850, and 720 cm^{-1}, as well as new bands originating from the ZIF-8 framework at 1420, 1310, 750, and 600 cm^{-1}. To verify that the ZIF-8 particles actually grew on the zeolite layers, the sample was evaluated with scanning electron microscopy (SEM). The recorded micrographs in Fig. 1(e) show that the IPC-1sw particles of around 25 × 50 μm^2 are covered by uniformly sized, cubic ZIF-8 nanoparticles of around 155 nm. These are formed solely on the IPC-1sw particles, and no unattached ZIF-8 particles could be observed. MOF growth occurred predominantly, but not exclusively, on the edges of the IPC-1sw particles, forming a fairly dense membrane [Fig. 2(b)]. This is important as it indicates that the nucleation of ZIF growth occurs primarily at the entrance to the interlayer region. This suggests that as soon as the Zn^{2+} ions emerge from the interlayer space, they coordinate with the linker molecules of the solution and quickly nucleate to form the ZIF-8 nanoparticles, resulting in successful MOF growth already after one addition cycle. While there are nanocrystals of ZIF-8 on the other surfaces of the IPC-1sw crystallites, they are more sparsely distributed than at the edges.

Moreover, it is noteworthy that the cubic ZIF-8 nanoparticles contrast with the typical morphology of ZIF-8 as truncated dodecahedral crystals, and according to the literature, this can be attributed to the presence of a modulating agent (such as the swelling agent $CTMA^+$) during the synthesis. Therefore, it is hypothesized that swelling agent $CTMA^+$ emerges from the zeolite interlayer space during the second synthesis step, which promotes the growth of the ZIF-8 nanoparticles to the zeolite surface. Similar behavior has been observed for the surfactant directed ZIF-8 growth on metal nanocrystals.[21,23,24] Thus, the hydrophobic chain of the surfactant attaches to the ZIF-8 nucleus, leading to growth on the zeolite

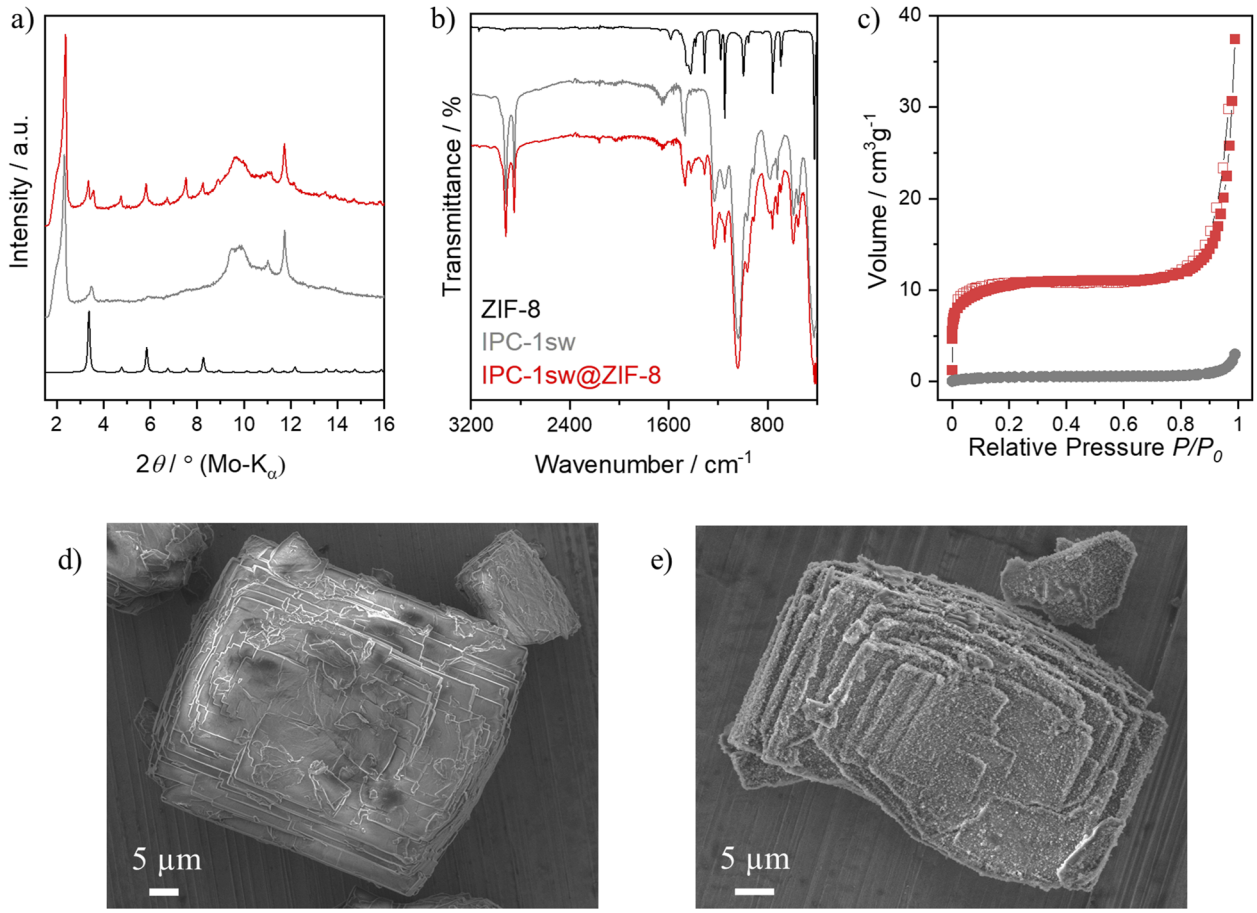

FIG. 1. Solid state characterization of ZIF-8 (black), IPC-1sw (gray), and IPC-1sw@ZIF-8 (red): (a) PXRD patterns, (b) FT-IR spectra, and (c) N_2 sorption analysis and SEM micrograph of IPC-1sw particles (d) before and (e) after successful ZIF-8 growth in H_2O:MeOH volume ratio of 9:1.

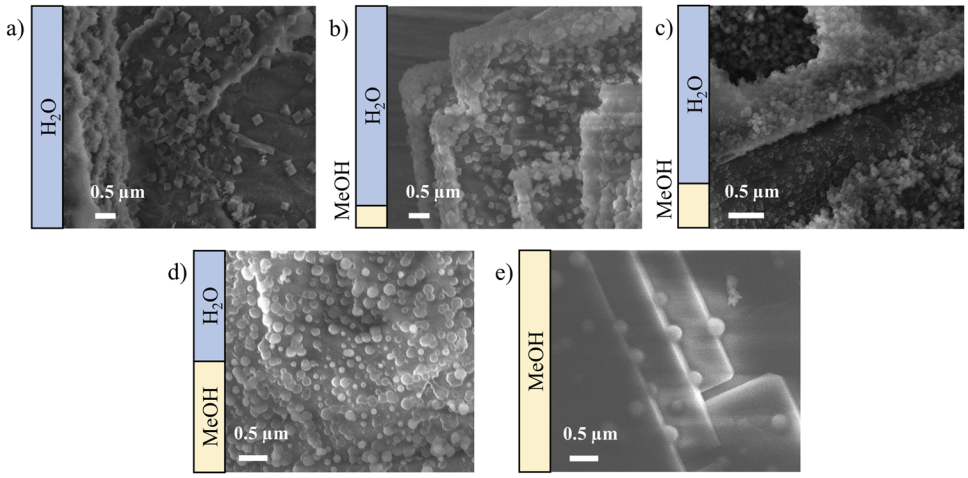

FIG. 2. Influence of the H_2O:MeOH solvent ratio on the ZIF-8 growth on IPC-1sw: (a) 10:0, (b) 9:1, (c) 8:2, (d) 5:5, and (e) 0:10.

surface. This happens predominately on the {100} facets of the ZIF-8 crystals, making them the crystal facet that determines the growth rate.[21,25] Consequently, a cubic morphology of the ZIF-8 particles is observed.[25] The importance of the swelling agent $CTMA^+$ during the ZIF-8 synthesis could be confirmed by applying the same protocol on the untreated zeolite precursor IPC-1P and the fact that no ZIF-8 growth was observed. The presence of both Zn^{2+} and the $CTMA^+$ pre-intercalated into the starting material region is important for the successful growth of the MOF primarily at the entrance to the interlayer region.

To further investigate the surface properties of the zeolite and their influence on the MOF growth, zeta potential measurements were performed. The initial surface of IPC-1P shows a negative zeta potential of −29.5 ± 3.0 mV, but this changes to a positive value of +22.6 ± 2.3 mV for IPC-1sw after swelling with $CTMA^+$. Therefore, the positively charged, surfactant covered surface of the zeolite enables the attachment of the ZIF-8 nanoparticles, which is consistent with the above proposed mechanism. The resulting zeta potential of IPC-1sw@ZIF-8 with +22.8 ± 0.2 mV is in good agreement with that of IPC-1sw, due to the positively charged ZIF-8 nanoparticles, which have a bulk value of +19.1 ± 0.7 mV.

The successful growth of ZIF-8 on the surface of ICP-1sw is also clearly reflected in the nitrogen sorption analysis [Fig. 1(c)]. Due to the swelling inside the pores of IPC-1sw, it only features a specific surface area as low as 2 $m^2\ g^{-1}$. However, this increases to 38 $m^2\ g^{-1}$ for IPC-1sw@ZIF-8. Moreover, the comparison of the pore size distribution of IPC-1sw and IPC-1sw@ZIF-8 indicates the presence of an additional pore around 11.8 Å, which can be attributed to ZIF-8.

B. Influence of the solvent ratio H_2O:MeOH

In order to modify the ZIF-8 growth with respect to size and morphology, different solvent compositions were investigated. It is well known that the solvent, e.g., water or methanol, plays an important role during the formation of ZIF-particles. Thus, different H_2O:MeOH volume ratios (10:0, 9:1, 8:2, 5:5, and 0:10) of the linker solution were systematically studied in order to investigate their influence on the growth of IPC-1sw@ZIF-8 hybrid materials. A successful ZIF-8 growth was obtained for smaller MeOH content from 10:0 to 5:5, where the addition of MeOH increases the amount of attached ZIF-8 (Fig. 2). However, in pure MeOH, only very broad and less intense reflections indicate a small amount and low crystallinity of the attached ZIF-8 particles. Furthermore, an increase of the MeOH content starts deswelling the IPC-1sw, as the $CTMA^+$ shows a higher solubility in alcoholic solution. Thus, the diminishing structural order along the crystallographic *a*-axis of the swollen zeolite can be seen by the very broad low angle reflection at ~2° 2θ (H_2O:MeOH = 5:5) to a complete absence of the reflection (0:10). This is in accordance with the decreasing band intensities of the $CTMA^+$ vibrations in the FT-IR spectrum.

The cubic morphology of the ZIF-8 nanoparticles could only be obtained for a small MeOH amount, due to the interaction with the $CTMA^+$ ions, as mentioned above. Herein, the small fraction was helpful to increase the total amount of ZIF-8 attaching to the zeolite as well as a more homogeneous morphology and size control. Moreover, the increase of MeOH decreases the average crystallite size from 185 (10:0), to 155 (9:1) to 63 nm (8:2) but also yields an overall better coverage of the zeolite particles (Fig. 2).

With higher MeOH content, the morphology changes to spherical ZIF-8 nanoparticles, as the $CTMA^+$ ions no longer interact with the MOF facets in organic solvents.[25] As a consequence, the attachment of the ZIF-8 nanoparticles via $CTMA^+$ bridging is not effective in methanolic solutions, resulting in a significant decrease in the number of ZIF-8 particles.

C. Influence on the number of additional steps

To evaluate the impact of multiple addition steps on the growth of ZIF-8 nanoparticles on the surface of IPC-1sw@ZIF-8, the number of additional steps was increased from one to three for the small MeOH ratios. Overall, one additional step includes loading the swollen zeolite with Zn^{2+} ions, removing excess ions, soaking it in the linker stock solution, and washing the final IPC-1sw@ZIF-8 hybrid material. The PXRD pattern shows an increase in intensity for the ZIF-8 related reflections for three addition steps, indicating an increase in ZIF-8 growth. This is in accordance with the slight

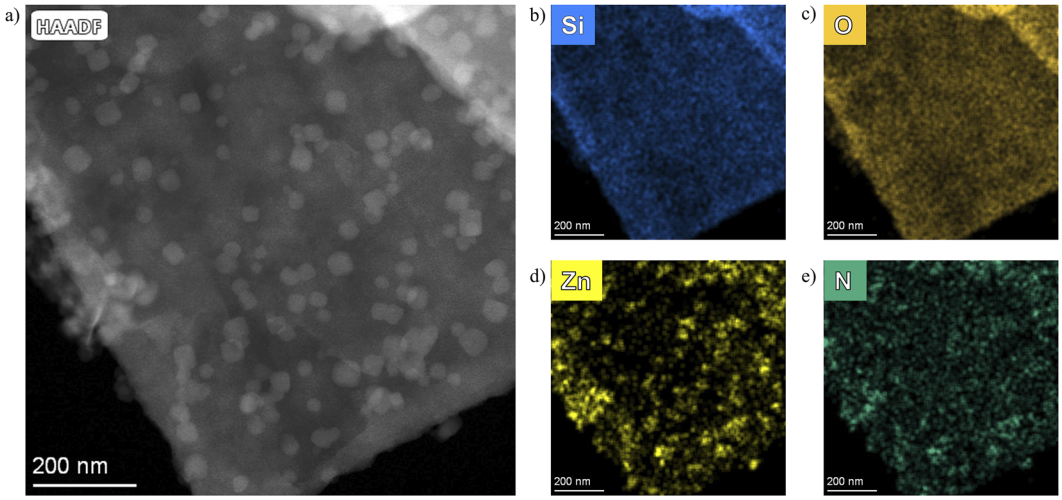

FIG. 3. EDS elemental mapping of CTMA-RUB-18@ZIF-8: (a) Dark field STEM image, and the compositional maps of (b) Si (blue), (c) O (orange), (d) Zn (light yellow), and (e) N (green); scale bar: 200 nm.

increase of the ZIF-8 related bands in the FT-IR spectra. However, the SEM images do not show continuous growth of ZIF-8 but rather selective growth of some particles. When using a H_2O:MeOH ratio of 9:1 for one addition step, the narrow particle size distribution of cubic ZIF-8 of around 155 nm broadens to a particle size distribution with bigger particles of 510 nm, a medium range of 285 nm, and a small fraction of 150 nm after three addition steps, reflecting the individual addition steps. The same holds for a H_2O:MeOH ratio of 8:2, where the particle size distribution shifts from one particle size of around 63 nm for one addition step to a bigger particle size distribution of 225, 160, and 90 nm after three addition steps. Besides the negative impact on the particle size distribution for both H_2O:MeOH ratios, the second and third addition steps also minimize the overall coverage of the IPC-1sw with ZIF-8 nanoparticles. Consequently, one addition step is best for achieving a narrow particle size distribution and homogeneous ZIF-8 growth on the entire IPC-1sw.

D. Transfer of the synthetic conditions to RUB-18

To prove the generality of the established ZIF-8 growth protocol on swollen 2D materials, Na-RUB-18 was chosen as an additional layered silicate. Na-RUB-18 was prepared according to the literature,[26] subsequently swollen with swelling agent $CTMA^+$[27] and the same protocol as for IPC-1sw was adopted. Similar to IPC-1sw, the PXRD shows the reflection of both the unchanged swollen CTMA-RUB-18 as well as newly formed ZIF-8. This could be confirmed by additional bands of ZIF-8 in the FT-IR spectrum. The SEM micrographs show the typical morphology of CTMA-RUB-18 square platelets with dimensions of about 2 μm and their coverage with cubic ZIF-8 nanoparticles of about 30–40 nm.

To visualize the element distribution, EDS elemental mapping was carried out (Fig. 3). The EDS mapping revealed that silicon and oxygen are homogeneously distributed within the silicate [Figs. 3(b) and 3(c)], whereas zinc can only be detected in the areas where small cubic ZIF-8 nanoparticles are attached to CTMA-RUB-18 [Fig. 3(d)]. Nitrogen, which is present in the ZIF-8 nanoparticles as well as the swelling agent $CTMA^+$, can be found with high intensity in the same areas as zinc and is homogeneously distributed within the CTMA-RUB-18 [Fig. 3(e)].

Also, in the case of Na-RUB-18, the zeta potential measurement revealed that the surface of the pristine silicate is negative at −52.8 ± 1.8 mV but results in a positive value of +10.5 ± 0.9 mV after swelling with $CTMA^+$. After growing ZIF-8 nanoparticles using a H_2O:MeOH ratio of 9:1, the resulting CTMA-RUB-18@ZIF-8 shows a slightly negative zeta potential at −3.9 ± 0.3 mV. This decreased value could be attributed to the fact that CTMA-RUB-18@ZIF-8 features a much smaller overall particle size than IPC-1sw@ZIF-8, which might accelerate the diffusion of $CTMA^+$ out of the zeolite during the ZIF-8 growth. Also, due to the much smaller particles of CTMA-RUB-18, there are probably fewer Zn^{2+} ions after the first step, so there is a smaller amount of Zn^{2+} for the subsequent ZIF-8 growth. In addition to this and/or as a result of this, ZIF-8 nanoparticles could only be grown on a smaller fraction of the surface of CTMA-RUB-18 compared to IPC-1sw.

Despite the relatively small fraction of ZIF-8, the nitrogen sorption analysis shows an increase in the specific surface area from 10 to 44 $m^2\ g^{-1}$ due to the presence of ZIF-8 on the surface of CTMA-RUB-18.

III. CONCLUSION

In this work, we could develop a new strategy for a controllable growth of ZIF-8 nanoparticles on swollen two-dimensional zeolites, in this case, IPC-1sw, which was obtained according to the ADOR mechanism by hydrolysis from Ge-UTL and a subsequent swelling with the surfactant $CTMA^+$. Hence, we could extend the ADOR concept toward novel hybrid materials, emphasizing the potential that this method provides in synthesizing novel materials.

The combination of the surfactant and the negatively charged zeolite layers enable the targeted MOF growth predominantly at the

entrance to the interlayer space on the surface of the zeolite. The ion exchange of the zinc ions in the zeolite layers thereby allows a controlled supply of Zn^{2+} ions for the formation and growth of the ZIF-8 nanoparticles after the addition of the linker solution. Consequently, already one addition cycle of metal ion and linker leads to the successful growth of ZIF-8. The surfactant in turn plays a crucial role in attaching the ZIF-8 nanoparticles, preferentially on the {100} facet, to the zeolite and, thus, also controlling their morphology toward uniformly sized nano cubes. We were able to show that the size and morphology can be fine-tuned by changing the solvent composition of water and methanol. To prove the concept, these findings were transferred to the layered and subsequently swollen silicate RUB-18, on which ZIF-8 was also successfully grown.

The protocol developed here shows a new interaction for MOF–zeolite hybrid materials, and these findings could help open new avenues for advanced hybrid materials. However, it is clear that the control over the growth of MOF particles on zeolite surfaces is complex, and in order to fully exploit the potential of MOF–zeolite hybrid materials, further research will be needed.

IV. EXPERIMENTAL SECTION

A. Synthesis of Ge-UTL

The structure directing agent (SDA) (6R,10S)-6,10-dimethyl-5-azoniaspiro[4.5]decane hydroxide was synthesized by adding 63 g (0.25 mol) of 1,4-dibromobutane over 30 min to a mixture of 28.3 g (0.25 mol) of 2,6-dimethylpiperidine, 41.5 g (0.3 mol) of K_2CO_3, and 250 ml of acetonitrile in a round bottom flask. After stirring overnight under reflux (16 h), K_2CO_3 is filtered off, acetonitrile is evaporated, and the resulting bromide salt is washed and filtered with diethyl ether. The hydroxide form is obtained using Ambersep 900(OH) ion exchange resin.

Ge-UTL is synthesized by hydrothermal synthesis.[28] In a typical synthesis, 3.14 g (30 mmol) of GeO_2 is dissolved in 47.3 ml (2625 mmol) of water, which contained 5.56 g (30 mmol) of SDA-OH. Subsequently, 3.60 g (60 mmol) of fumed silica (Cab–O–Sil) is added and stirred for 30 min. The resulting gel is transferred to a Teflon-lined stainless-steel autoclave and heated at 175 °C for seven days. The product was filtered, washed with water, and dried overnight at 80 °C. To remove the SDA, the product was calcined at 550 °C for 6 h in air.

B. Preparation of IPC-1P

The lamellar precursor IPC-1P was synthesized by hydrolyzing 1 g of calcined Ge-UTL in 200 ml of 0.1M HCl at 90 °C for 16 h under reflux. The product was filtered, washed with water, and dried at 80 °C overnight.

C. Preparation of IPC-1sw

0.3 g of IPC-1P was dispersed in a mixture of 13.5 g of 25 wt. % CTMA-Cl and 1.5 g of 40 wt. % TPA-OH and stirred for 16 h. The product was isolated by centrifugation, washed twice with water, and dried at 60 °C overnight.

D. Preparation of IPC-1sw@ZIF-8

0.1 g of IPC-1sw is dispersed in 10 ml of a 0.1M $Zn(NO_3)_2$ aqueous solution and stirred for 1 h. The solid is recovered by centrifugation (9000 rpm, 5 min) and washed twice to remove excess Zn^{2+} ions. Subsequently, 10 ml of a 0.1M 2-MeIm solution (H_2O, MeOH, or mixture) is added and stirred for 1 h. The particles are recovered as in the previous step and dried at 80 °C. If noted, this procedure is repeated two more times.

E. Synthesis of Na-RUB-18

Na-RUB-18 was synthesized according to the literature procedure.[26] 7.105 g of $Na_2SiO_3{\cdot}9H_2O$ is added to a mixture of 11.265 g of colloidal silica (Ludox As-40) and 0.809 g of water. After mixing for 15 min, the fluid gel is transferred to a Teflon-lined stainless-steel autoclave and heated at 100 °C for 20 days. The product is filtered, washed with water, and dried at 80 °C overnight.

F. Preparation of CTMA-RUB-18

The swelling of Na-RUB-18 was performed similarly to the literature.[27] 1.14 g of Na-RUB-18 was added to 23 ml of an aqueous solution containing 2.944 g of 25 wt. % CTMA-Cl and 0.153 g of 40 wt. % TPA-OH. The suspension is stirred at 80 °C under reflux for 3 h, transferred to a Teflon-lined stainless-steel autoclave, and heated at 150 °C for two days. The swollen CTMA-RUB-18 was filtered, washed, and dried at room temperature overnight.

G. Preparation of CTMA-RUB-18@ZIF-8

The same protocol as for the IPC-1sw@ZIF-8 particles was applied, except for the usage of 0.5M concentrations for the metal and linker solution.

H. Structural Characterization

Powder x-ray diffraction (PXRD) patterns were recorded on STOE STADI/P diffractometer using Mo $K_{\alpha 1}$ radiation (λ = 0.70930 Å) at room temperature operated in capillary Debye–Scherrer mode. FTIR spectroscopy was carried out using a Shimadzu IR Affinity-1 FTIR spectrophotometer in transmittance mode from 400 to 4000 cm^{-1}. SEM micrographs were collected using a IT800 at a working distance of 4 mm and low operating voltages (3–5 kV) to ensure sensitive mapping of the surface. Samples were prepared by depositing a drop of powdered sample dispersed in ethanol onto copper tape prior to recording. TEM micrographs were obtained using a FEI Titan Themis operated at 200 kV on samples prepared by deposition of one drop of nanoparticle suspension on holey carbon films supported on a 300 mesh Cu grid (Agar Scientific®). The Zeta potential was measured in water and at room temperature using a Malvern Zetasizer μV instrument (Malvern Panalytical, UK).

I. Gas adsorption

BET-specific surface area determination from N_2 isotherms was carried out according to the Rouquerol theory[29] using the Microactive Software Kit v4.03.04. Data were recorded on a Micromeritics Tristar ii Surface Area and Porosity Instrument.

Samples (~100 mg) were added to a frit tube and activated *in vacuo* (100 °C, ~3 × 10^{-5} mbar, 16 h) prior to the measurement.

ACKNOWLEDGMENTS

The authors would like to thank the European Research Council for funding opportunities under Advanced Grant No. 787073. The EPSRC Light Element Analysis Facility under Grant No. EP/T019298/1 and the EPSRC Strategic Equipment Resource under Grant No. EP/R023751/1 are gratefully acknowledged.

AUTHOR DECLARATIONS

Conflict of Interest

The authors have no conflicts to disclose.

Author Contributions

Philip Netzsch: Conceptualization (equal); Data curation (equal); Resources (lead); Writing – original draft (equal); Writing – review & editing (equal). **Romy Ettlinger**: Data curation (equal); Writing – original draft (equal); Writing – review & editing (equal). **Russell E. Morris**: Conceptualization (equal); Funding acquisition (lead); Project administration (lead); Supervision (lead); Writing – original draft (equal); Writing – review & editing (equal).

DATA AVAILABILITY

The research data supporting this publication can be accessed at https://doi.org/10.17630/b59b1ac2-78d8-47eb-82ba-996139e0b51d.

REFERENCES

[1] Y. Li and J. Yu, Nat. Rev. Mater. **6**, 1156 (2021).
[2] S. Kulprathipanja and R. B. James, *Zeolites in Industrial Separation and Catalysis* (WileyVCH, Weinheim, 2010).
[3] R. Freund, O. Zaremba, G. Arnauts, R. Ameloot, G. Skorupskii, M. Dincă, A. Bavykina, J. Gascon, A. Ejsmont, J. Goscianska, M. Kalmutzki, U. Lächelt, E. Ploetz, C. S. Diercks, and S. Wuttke, Angew. Chem., Int. Ed. **60**, 23975 (2021).
[4] R. Freund, S. Canossa, S. M. Cohen, W. Yan, H. Deng, V. Guillerm, M. Eddaoudi, D. G. Madden, D. Fairen-Jimenez, H. Lyu, L. K. Macreadie, Z. Ji, Y. Zhang, B. Wang, F. Haase, C. Wöll, O. Zaremba, J. Andreo, S. Wuttke, and C. S. Diercks, Angew. Chem., Int. Ed. **60**, 23946 (2021).
[5] P. Rani, V. Kasneryk, and M. Opanasenko, Appl. Mater. Today **26**, 101283 (2022).
[6] Q. Al-Naddaf, H. Thakkar, and F. Rezaei, ACS Appl. Mater. Interfaces **10**, 29656 (2018).
[7] D.-W. Lim, H. Lee, S. Kim, I. H. Cho, M. Yoon, and Y. N. Choi, Chem. Commun. **52**, 6773 (2016).
[8] J. Peng, Y. Li, X. Sun, C. Huang, J. Jin, J. Wang, and J. Chen, ACS Appl. Mater. Interfaces **11**, 4328 (2019).
[9] J. Peng, X. Sun, Y. Li, C. Huang, J. Jin, Dhanjai, J. Wang, and J. Chen, Microporous Mesoporous Mater. **268**, 268 (2018).
[10] D. Suttipat, W. Wannapakdee, T. Yutthalekha, S. Ittisanronnachai, T. Ungpittagul, K. Phomphrai, S. Bureekaew, and C. Wattanakit, ACS Appl. Mater. Interfaces **10**, 16358 (2018).
[11] W. J. Roth, P. Nachtigall, R. E. Morris, and J. Čejka, Chem. Rev. **114**, 4807 (2014).
[12] U. Díaz and A. Corma, Dalton Trans. **43**, 10292 (2014).
[13] A. Corma, U. Díaz, T. García, G. Sastre, and A. Velty, J. Am. Chem. Soc. **132**, 15011 (2010).
[14] M. Opanasenko, M. Shamzhy, F. Yu, W. Zhou, R. E. Morris, and J. Čejka, Chem. Sci. **7**, 3589 (2016).
[15] W. J. Roth, B. Gil, A. Mayoral, J. Grzybek, A. Korzeniowska, M. Kubu, W. Makowski, J. Čejka, Z. Olejniczak, and M. Mazur, Dalton Trans. **47**, 3029 (2018).
[16] W. J. Roth, B. Gil, W. Makowski, B. Marszalek, and P. Eliášová, Chem. Soc. Rev. **45**, 3400 (2016).
[17] P. Eliášová, M. Opanasenko, P. S. Wheatley, M. Shamzhy, M. Mazur, P. Nachtigall, W. J. Roth, R. E. Morris, and J. Čejka, Chem. Soc. Rev. **44**, 7177 (2015).
[18] W. J. Roth, P. Nachtigall, R. E. Morris, P. S. Wheatley, V. R. Seymour, S. E. Ashbrook, P. Chlubná, L. Grajciar, M. Položij, A. Zukal, O. Shvets, and J. Čejka, Nat. Chem. **5**, 628 (2013).
[19] M. Opanasenko, W. O. Parker, M. Shamzhy, E. Montanari, M. Bellettato, M. Mazur, R. Millini, and J. Čejka, J. Am. Chem. Soc. **136**, 2511 (2014).
[20] P. Chlubná, W. J. Roth, H. F. Greer, W. Zhou, O. Shvets, A. Zukal, J. Čejka, and R. E. Morris, Chem. Mater. **25**, 542 (2013).
[21] G. Zheng, Z. Chen, K. Sentosun, I. Pérez-Juste, S. Bals, L. M. Liz-Marzán, I. Pastoriza-Santos, J. Pérez-Juste, and M. Hong, Nanoscale **9**, 16645 (2017).
[22] M. Shamzhy, M. Mazur, M. Opanasenko, W. J. Roth, and J. Čejka, Dalton Trans. **43**, 10548 (2014).
[23] P. Hu, J. Zhuang, L.-Y. Chou, H. K. Lee, X. Y. Ling, Y.-C. Chuang, and C.-K. Tsung, J. Am. Chem. Soc. **136**, 10561 (2014).
[24] G. Zheng, S. de Marchi, V. López-Puente, K. Sentosun, L. Polavarapu, I. Pérez-Juste, E. H. Hill, S. Bals, L. M. Liz-Marzán, I. Pastoriza-Santos, and J. Pérez-Juste, Small **12**, 3935 (2016).
[25] Y. Pan, D. Heryadi, F. Zhou, L. Zhao, G. Lestari, H. Su, and Z. Lai, CrystEngComm **13**, 6937 (2011).
[26] K. Endo, Y. Sugahara, and K. Kuroda, Bull. Chem. Soc. Jpn. **67**, 3352 (1994).
[27] H. F. Greer, W. Zhou, N. Alam, and R. Mokaya, J. Mater. Chem. **22**, 23141 (2012).
[28] O. V. Shvets, A. Zukal, N. Kasian, N. Žilková, and J. Čejka, Chem. Eur. J. **14**, 10134 (2008).
[29] J. Rouquerol, P. Llewellyn, and F. Rouquerol, Stud. Surf. Sci. Catal. **160**, 49 (2007).